


Article

Autonomous Fever Detection, Medicine Delivery, and Environmental Disinfection for Pandemic Prevention

Chien-Yu Su * and Kuu-Young Young

Department of Electrical Engineering, National Yang Ming Chiao Tung University, 1001 University Road, Hsinchu 300, Taiwan; kyoung@nycu.edu.tw

* Correspondence: drjerrysu@gmail.com

Abstract: In facing the outbreak of the pandemic, robots are highly appealing for their non-contact nature. Among them, we have selected the mobile robot manipulator to develop an autonomous system for pandemic prevention, as it possesses both mobility and manipulability. The robot was used as a platform for performing autonomous fever detection, medicine delivery, and environmental disinfection system for the fever station and isolation ward, which are the two primary units that deal with the pandemic in a hospital. The proposed novel algorithms aim to ensure both human safety and comfort by automating fever detection and recognizing medicine taking. Additionally, they address environmental disinfection by effectively covering blind spots. We conducted a series of experiments to evaluate their performance in a hospital-like setting, which was designed specifically for the testing of intelligent medical systems developed in our university. Quantitative assessment was administered to analyze how the introduction of the proposed autonomous system reduced the risk of infection, and feedback was also collected from participants through questionnaires.

Keywords: pandemic prevention; fever detection; medicine delivery; environmental disinfection; mobile robot manipulator



Citation: Su, C.-Y.; Young, K.-Y. Autonomous Fever Detection, Medicine Delivery, and Environmental Disinfection for Pandemic Prevention. *Appl. Sci.* **2023**, *13*, 13316. <https://doi.org/10.3390/app132413316>

Academic Editors: Carlo Ferraresi, Carlo De Benedictis and Guido Danieli

Received: 17 November 2023

Revised: 13 December 2023

Accepted: 15 December 2023

Published: 17 December 2023



Copyright: © 2023 by the authors. Licensee MDPI, Basel, Switzerland. This article is an open access article distributed under the terms and conditions of the Creative Commons Attribution (CC BY) license (<https://creativecommons.org/licenses/by/4.0/>).

1. Introduction

Robots have been applied in various medical fields for some time. Early applications included minimally invasive surgery and the da Vinci robot [1]. Anthropomorphic and zoomorphic robots have been utilized in the treatment of children with autism [2], while companion robots assist cognitively impaired elderly individuals living alone at home [3]. Recently, due to the immense impact caused by the global COVID-19 pandemic outbreak, replacing humans with robots has gained attention due to the ability to reduce disease transmission, shortages in personal protective equipment, and consumption of medical resources, in addition to the protection of medical staff [4]. Among various types of robots, the mobile robot manipulator is of focus for its ability to combine both mobility and manipulability. For instance, Conte et al. [5] proposed using the mobile manipulator to carry the ultraviolet germicidal lamp for disinfection. Mišeikis et al. [6] applied it for disinfection and remote body temperature detection. Motivated by its noncontact nature and flexibility, we thus propose developing an autonomous fever detection, medicine delivery, and environmental disinfection system based on using a mobile robot manipulator for the fever station and isolation ward in a hospital, as they are regarded as the high-risk areas for pandemic prevention [7].

For the function of fever detection, the proposed system allows the robot to adjust its posture to accommodate individuals of different heights for temperature measurement, and it is also connected to a real-name system for tracking purposes. While the motion planning and governing involved in this task is not so complicated, as demonstrated in previous research [8–10], the proposed approach further emphasizes human safety and comfort, as the robot may interact with humans during the measurement process. In related research,

Nakhaeina et al. [11] developed a compliant wrist to support robotic interaction with real-time proximity and contact feedback to ensure the collaborator's safety. Lasota et al. [12] proposed attaching a wearable sensor on a human for the robot to detect and then avoid collision via speed adjustment. We propose regulating the speed of the robot toward a person according to their relative distance [13], as well as providing a voice reminder.

In response to the situation of a certain percentage of patients not adhering to the medication regimen, which results in a large number of preventable deaths and a huge waste of healthcare resources [14,15], the proposed system will further check whether the medicines are indeed taken by the patients by monitoring their motions after medicine delivery. In previous research, Yang et al. proposed applying remote control for robot-assisted medication delivery via healthcare personnel [4]. Lee and Youm proposed utilizing a wearable watch to collect users' medication images, which were then uploaded to a cloud server for analysis [16]. Jun et al. proposed applying the gated recurrent unit-based neural network to classify 3D human skeletons in determining whether the medicines have been taken [17]. Further, Osawa, Huang, and Yu proposed using the Support Vector Machine (SVM) to classify depth images of hand motions during medication intake [18]. To serve as an autonomous system that is free of privacy concerns, the proposed approach aims to recognize the action of medicine taking from the corresponding arm motion sequence. We chose that of the arm over the hand, as it may be less affected by clothes and others. A novel algorithm named the Segmented Dynamic-Time-Warps Recognizer (SDTWR) was then proposed based on the concept of dynamic time warps [19], which is frequently used for measuring similarity between two temporal sequences. Both the Support Vector Machine (SVM) and Convolutional Neural Network (CNN) are considered effective for time series recognition and are potential candidates for serving as the learning mechanism. However, during our preliminary study, the CNN demonstrated superior performance.

Environmental disinfection is very crucial for the safety and health of medical staff and patients. It needs to be conducted regularly and also under request. In previous research, Conte, Leamy, and Furukawa proposed installing Ultraviolet-C (UVC) lamps on the robot itself and also on the robotic arm to allow for more comprehensive disinfection, while it required human intervention for remote control [5]. Tiseni et al. proposed using the genetic algorithm to plan the path for a mobile robot equipped with the UVC lamp [20], although they focused more on robot trajectory planning for disinfection. Sanchez and Smart proposed an approach that considered the shapes of the objects in the environment, although they were limited to those with flat and unobstructed surfaces [21]. Based on the discussions above, we thus propose a novel approach for disinfection so that a more thorough and even disinfection can be achieved for all kinds of objects in a 3D environment, along with an assessment of the UVC irradiation intensity for validation of homogenous disinfection.

With the introduction of the proposed autonomous system, it is expected that the risk of infection should be alleviated, which will be evaluated by the proposed quantitative assessment method. For demonstration, this system was applied to a series of experiments by navigating the robot through task execution in a smart ward, which is a hospital-like setting designed specifically for evaluating intelligent medical systems developed in our university. Questionnaires based on the system usability scale were also administered to obtain subjects' feedback [22].

Compared with previous approaches, we consider that the proposed system has the following merits:

- Novel algorithms for automatic fever detection and medicine-taking recognition that ensure both human safety and comfort, as well as environmental disinfection that covers blind spots well, were developed.
- A quantitative assessment method for evaluating the reduction in infection risk through the use of robots based on the duration and proximity of contact with confirmed cases was developed.

- Via integration with multi-sensors and a collision-free path planning strategy, an autonomous system that was capable of navigating the mobile robot manipulator among static obstacles and moving people was developed and applied for a field study in a hospital-like environment.

The rest of this paper is organized as follows: Section 2 describes the proposed system, including the modules for pose and action recognition, control strategy, environmental disinfection, and infection risk assessment. Section 3 presents the experimental results conducted in our university smart ward, along with the results of infection risk assessment and the analysis of questionnaire surveys from the subjects. Finally, concluding remarks are given in Section 4.

2. Proposed System

Figure 1 shows the conceptual diagram of the proposed fever detection, medicine de-livery, and environmental disinfection system. It includes the modules of posture and action recognition, disinfection, safety control, infection risk assessment, navigation, and real-name system. The proposed system is activated when a person arrives at the fever station. With the information from the depth camera, it first utilizes the function of posture recognition described in Section 2.1 to make sure he/she is ready for temperature measurement, and then proceeds with the subsequent operations corresponding to the fever status. To serve for medicine delivery to the patients allocated in the isolation ward, it demands the function of navigation to move between the fever station and isolation ward, as well as posture and action recognition to judge whether the patient has actually taken the medicine. For the safety and comfort of the persons involved in the processes, the system monitors the distance between the human and the robot and then executes corresponding safety control, as described in Section 2.2. Disinfection of the fever station and isolation ward is conducted to ensure their hygiene under a regular basis or under request. The proposed strategy, which is capable of achieving an even disinfection effect for all the objects in the environment, is described in Section 2.3. To evaluate how the risk of infection can be alleviated due to the introduction of the proposed system, we came up with a method for quantitative assessment based on contact time and distance in a contagious environment, described in Section 2.4. Data collected by the thermometer and depth camera are linked to the real-name system for further analysis and utilization, as described in Section 2.5.

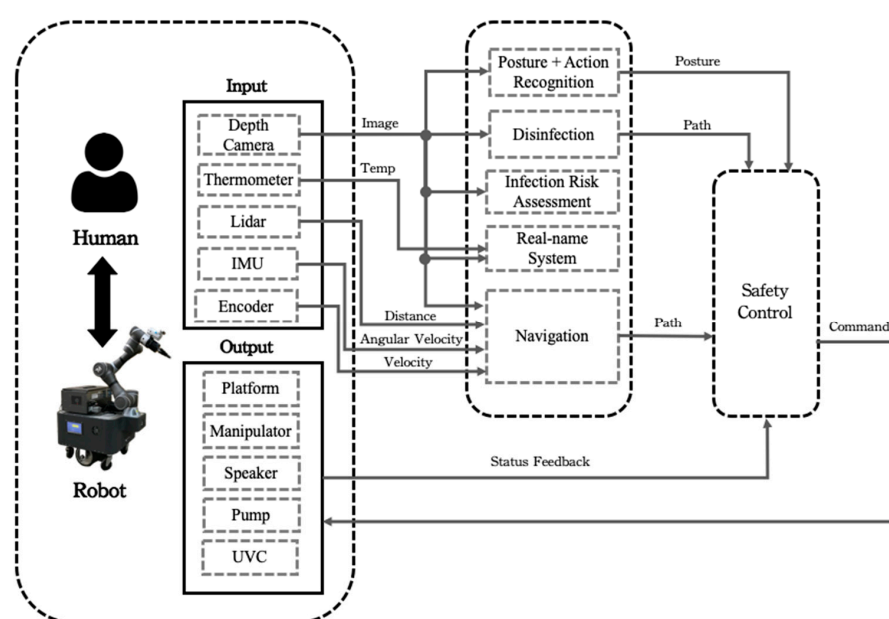


Figure 1. Conceptual diagram of the proposed fever detection, medicine delivery, and environmental disinfection system.

Navigation and control of the mobile robot manipulator follows that which was developed in our previous research [23]. Three kinds of sensors are adopted for position and orientation measurement, including Lidar, inertial measurement unit (IMU), and encoder. The A* algorithm is used for global path planning among static obstacles, and the dynamic window approach is used for avoiding moving staff and pedestrians [23]. Details of its implementation are referenced in [23]. Meanwhile, voice reminders are provided through a speaker to assist with temperature measurement and medicine delivery, a pump is used for alcohol disinfection, and UVC lamps are used for environmental disinfection.

2.1. Posture and Action Recognition

Posture recognition is used to determine the readiness of a person for temperature measurement in the fever station, as well as the measurement location on his/her forehead. Meanwhile, it is also utilized to detect whether a patient has actually taken the medicine in the isolation ward according to his/her arm motions. The system initially captures images using the depth camera and subsequently feeds them into the OpenPose algorithm, a renowned method for 2D human skeleton identification and processing [24]. As one example of posture analysis, shown in Figure 2, 25 key joint points on the human body are identified. The system then uses the point cloud information for depth Z_i , also obtained from the depth camera, to derive the 3D coordinates (X_i, Y_i, Z_i) for point i from its corresponding 2D coordinates (x_i, y_i) , which are represented in the coordinate system of the camera, as described in (1):

$$\begin{bmatrix} X_i \\ Y_i \\ Z_i \end{bmatrix} = Z_i \begin{bmatrix} f_x & s & c_x \\ 0 & f_y & c_y \\ 0 & 0 & 1 \end{bmatrix}^{-1} \begin{bmatrix} x_i \\ y_i \\ 1 \end{bmatrix} \quad (1)$$

where (c_x, c_y) , (f_x, f_y) , and s are the center coordinates of the image, focal lengths expressed in pixels, and a scale factor, respectively, and the unit is meters. We use the neck, hip, and knee locations out of the 25 key points to check whether the person has already sat still for temperature measurement, as well as the shoulder, elbow, and wrist for the action of medicine taking.

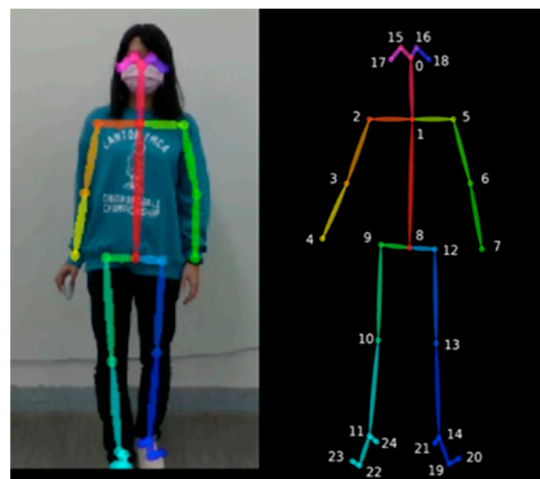


Figure 2. An example of posture analysis involves the assessment of the human body using 25 key joint points.

As the recognition of a sitting posture is relatively straightforward, it can be determined by simply inspecting whether the angle between neck-to-hip and hip-to-knee is close to 90° for a period of time. On the other hand, the checking of medicine-taking action is more challenging, as it demands the analysis of the time sequence corresponding to the entire action, while there may exist slight differences in motion not only for different

persons, but even for the same one. In response, we propose a novel algorithm, SDTWR, based on the concept of dynamic time warps [19], frequently employed for evaluating the similarity between two temporal sequences of different speeds and found to be effective in applications such as speech and handwriting recognition, as well as motion analysis.

The SDTWR operates as follows. First, the time sequence of the medicine-taking action acquired via the depth camera is taken as the input. For each sample on the sequence, the shoulder, elbow, and wrist locations of the arm are grouped together to form a set S_i that represents a posture, expressed as

$$S_i = \begin{bmatrix} J_{i, s} \\ J_{i, e} \\ J_{i, w} \end{bmatrix} = \begin{bmatrix} X_{i,s} & Y_{i,s} & Z_{i,s} \\ X_{i,e} & Y_{i,e} & Z_{i,e} \\ X_{i,w} & Y_{i,w} & Z_{i,w} \end{bmatrix} \tag{2}$$

where $J_{i, s}$, $J_{i, e}$, and $J_{i, w}$ represent the 3D coordinates of the shoulder, elbow, and wrist, respectively. For S_i among a total number of m training sets, it needs to be normalized to become S_{N_i} :

$$S_{N_i} = \frac{S_i - \min_{1 \leq i \leq m} \{S_i\}}{\max_{1 \leq i \leq m} \{S_i\} - \min_{1 \leq i \leq m} \{S_i\}} \tag{3}$$

Consequently, the action of medicine taking can then be viewed as the combination of a series of S_N . To achieve a better recognition effect, the entire medicine-taking action (MTA) is further divided into five sub-actions according to evident differences between them, as shown in Figure 3. To acquire the typical MTA as the reference, we invited 10 subjects and asked each of them to conduct the MTA three times. These 30 collected time sequences, pre-processed via (3) to become that of S_N , were then sent to the CNN for training and classification. We adopted the CNN over SVM as the learning mechanism for its better recognition rate for this application [25,26]. Finally, the posture sequence $R = [A, B, C, D, E]$ was generated to serve as a standard MTA. To judge whether the patient had actually taken the medicine, the corresponding time sequence was first recorded and processed to become posture sequence $O = [o_1, \dots, o_m]$ of m samples. They were then forwarded to the CNN to determine which sub-action among $\{A, B, C, D, E\}$ a given o_i should belong to. Because R and O_l (O with postures labeled) might not be the same length due to different motion speeds, the method of dynamic time warps was utilized to evaluate their similarity [19]. An $m \times 5$ matrix M was then generated, expressed as

$$M_{m \times 5} = \begin{bmatrix} M(1,1) & \dots & \dots & M(1,5) \\ \vdots & M(i-1,j-1) & M(i-1,j) & \vdots \\ \vdots & M(i,j-1) & M(i,j) & \vdots \\ M(m,1) & \dots & \dots & M(m,5) \end{bmatrix} \tag{4}$$

where $M(i, j)$ is the so-called dynamic time warping distance when the i posture of O_l is aligned with the j posture of R , derived using an optimal alignment scheme in the algorithm of dynamic time warping [19] so that the similarity can be evaluated for R and O_l , even when their timing is different. When the derived similarity measurement value from the process falls below an empirically selected threshold, they are deemed to be similar. Based on the discussions above, the algorithm developed for medicine-taking detection is organized as follows:

Algorithm for medicine-taking detection to determine whether the patient has taken the medicine from the measured time sequence of his/her arm motion:

- Step 1: Input the patient’s time sequence of medicine taken, measured via the depth camera, and process it to become the posture sequence O . Classify the postures into corresponding sub-actions A~E via the CNN and rename O to be O_l .

- Step 2: Obtain the standard posture sequence R to serve as the reference for comparison from a number of demonstrations of successful medicine taking.
- Step 3: Generate Matrix M for similarity evaluation between R and O_l . Derive the dynamic time warping distance for its elements $M(i,j)$ for similarity measurement.
- Step 4: If the value of the similarity measurement in Step 3 is smaller (larger) than a preset threshold, the patient is judged to have (not) taken the medicine.

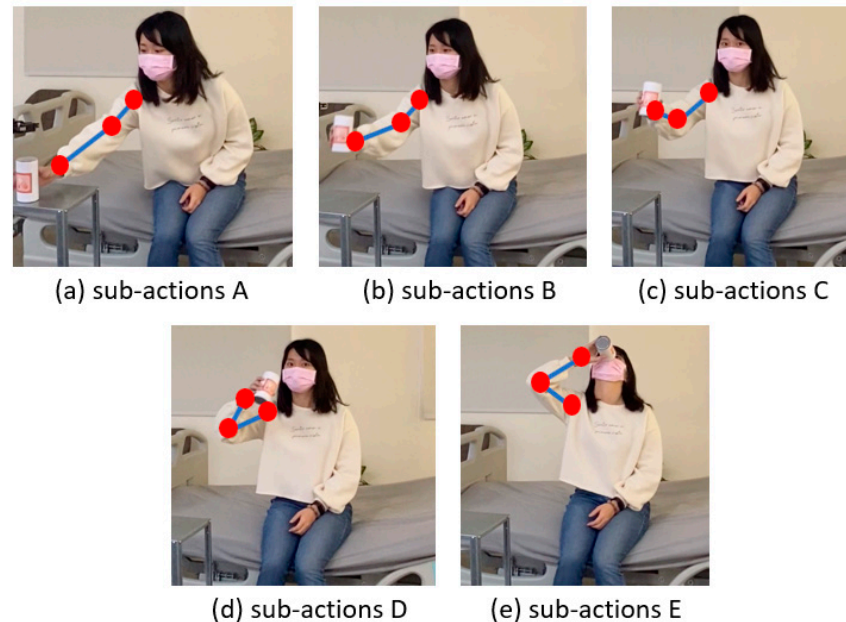


Figure 3. The medication-taking action is further divided into five sub-actions.

In response to non-compliant patients, the robot follows a series of steps. Initially, the robot utilizes an integrated speaker system to repeatedly play voice prompts, encouraging patient cooperation. If the patient continues to be unresponsive, the robot will automatically send a notification to the nursing station, alerting healthcare professionals. To further manage the situation, nurses can engage in real-time communication with the patient using a microphone. Additionally, the system allows nurses to remotely control the robot through a WiFi connection. During manual operation, the robot's camera streams visual content in real-time to the nurse's interface. When the robot is unable to complete the assigned task, it sends an error message to the nursing station, requesting remote control intervention by personnel.

2.2. Safety Control

By taking into account both the safety and comfort of a person in the presence of the robot during task execution [27,28], the system conducts speed control based on their relative distance. It regulates robot speed according to the distance between a person and a robot, as shown in Figure 4 [23]. The robot halts completely when it enters the region in red, which is set to be 0.13 m and 1.3 m for temperature measurement and medicine delivery, respectively, and decreases its speed when it is within the region in yellow, set to be 0.4 m and 1.7 m as the warning regions; otherwise, a normal speed is maintained, although these distances are subject to robot speed and other considerations. To achieve a smooth transition from the initial normal speed V_{ini} to an adjusted deceleration speed V_{adj} , a sigmoid function U , shown in Figure 5, is utilized, as described in (5):

$$V_{adj} = U(D) \times V_{ini} \quad (5)$$

where D is the distance between the person and the robot. D_{dec} is for deceleration, and D_{stop} is for stopping.

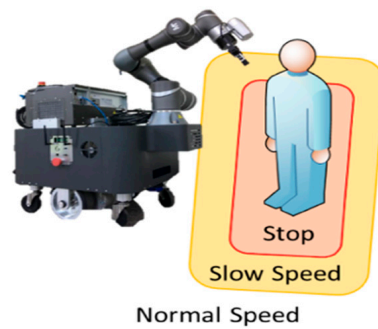


Figure 4. Speed regulation according to the distance between human and robot.

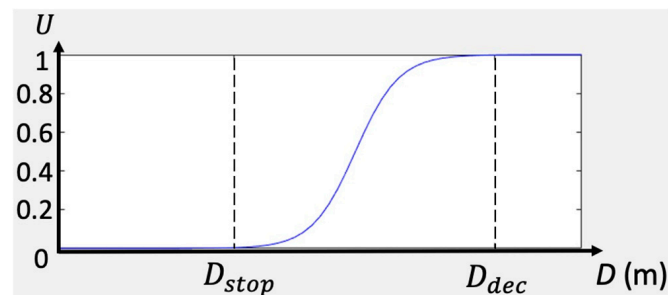


Figure 5. Speed smoothing between normal navigation, deceleration, and full stop.

In addition to speed control, to further raise the comfort and expectation of the subjects during temperature measurement, the system will also constrain the approaching direction of the robot arm toward his/her forehead. As shown in Figure 6, the robot arm is constrained to move toward the subject's forehead in a direction within a 60° range. To achieve it, the system will search for joint solutions corresponding to the points on the approaching path that satisfy this directional requirement. Based on the discussions above, the algorithm developed for temperature measurement is organized as follows:

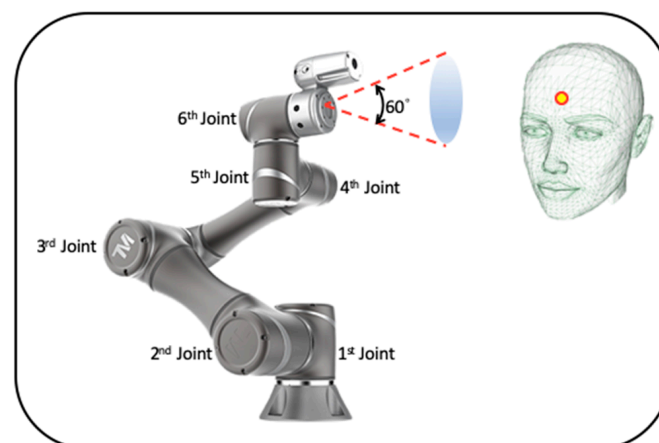


Figure 6. The robotic arm is regulated to approach the human's forehead within a 60° range of orientation.

Algorithm for temperature measurement, restricting the end-effector orientation of the robotic arm and adjusting speed based on distance for patient safety and comfort:

- Step 1: Confirm that the patient is seated and stationary.
- Step 2: Utilize the depth camera on the robotic arm to calculate the coordinates of the patient's forehead.
- Step 3: Compute the path from the robotic arm to the forehead and restrict the orientation of the end-effector.
- Step 4: Dynamically adjust the arm's speed based on the distance from the patient.

2.3. Environmental Disinfection

The CONNOR UVC Disinfection Robot [29], Xenex Disinfection Services LightStrike [30], TmiRob [31], XDBOT [32], and Siemens and Aucma Co., Ltd's disinfection robots [33] represent existing commercial disinfection systems. In comparison to these systems, our solution offers several advantages. We utilize 3D cameras to create detailed maps of the environment. Beyond having UVC lights on the robot's body, our system is equipped with UVC lights on a six-axis robotic arm, allowing for flexible and precise surface coverage, especially in complex environments. Moreover, we introduce a dosage estimation method to achieve uniform and effective disinfection by spreading appropriate dosage to each area.

The proposed system aims to achieve even disinfection for the entire environment, which is then validated via the assessment of UVC irradiation dose. The UVC lamps are equipped on both the mobile platform and robotic arm of the mobile robot manipulator, with the former used for disinfection in the open area and the latter for objects with complex surface contours that usually lead to blind spots. Therefore, the proposed system should enable the mobile robot manipulator to autonomously explore unknown environments and objects, build the corresponding maps for both the mobile platform and the robotic arm, and then segment them for path planning, obstacle avoidance, and object contour following.

Figure 7 shows the system block diagram for environmental disinfection. As the navigation of the mobile platform is applied to the open area, the system utilizes the Lidar and the technique of 2D SLAM to obtain a 2D map of the environment, which is then sent to the developed navigation scheme for path planning [23]. The GMapping algorithm is adopted to serve for 2D SLAM, as it is effective and accurate enough for this application [34]. The robotic arm is activated when an object in the environment is detected. To let it be able to follow the contour of the object for disinfection, the system utilizes the depth camera and that of 3D SLAM to derive a 3D map. The Real-Time Appearance-Based Mapping (RTABMap) algorithm is adopted for 3D SLAM [35], which fits well with the 3D data acquired from the depth camera. Figure 8 illustrates the process of constructing a map for a laboratory environment using RTABMap. Specifically, Figure 8a displays the input captured using the depth camera, while Figure 8b exhibits the resulting point cloud map. With the 3D map available, the system then adopts the Probabilistic Roadmap (PRM) and Nearest Neighboring (NN) algorithms to determine an effective and collision-free disinfection path, among several possible choices [36,37].

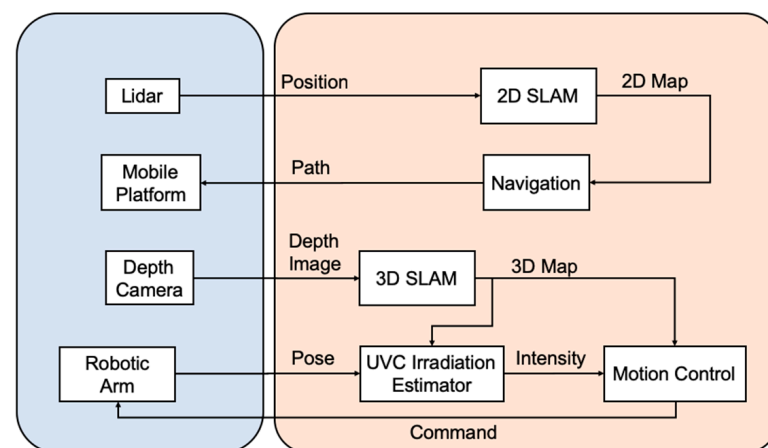


Figure 7. System block diagram for environmental disinfection.

To ensure that the UVC irradiation is enough for the entire object, the robotic arm will stay on the same location of the path until the estimated intensity reaches the preset amount. We came up with a method for estimation based on that in [38], while further considering the pose of the UVC lamps so that the effect due to the incident angle of the irradiation can also be included in computing the received intensity on the surface, as

described below. For each point light source along the UVC lamp, the generated irradiation dE can be derived as

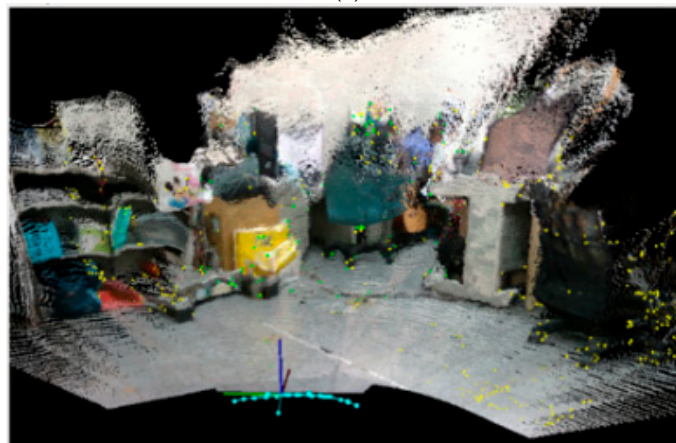
$$dE = \frac{\Phi_E}{4\pi L} \frac{1}{(x^2 + y^2 + (z - \ell)^2)} d\ell \hat{r} \cdot \hat{n} \quad (6)$$

where the center of the lamp is set to be the origin, its length and irradiation intensity are denoted as L and Φ_E , respectively, the point light source and its distance to the origin are denoted as $d\ell$ and ℓ , the vector from the point light source to the point $r(x, y, z)$ under estimation is denoted as \hat{r} , and the unit normal vector of r is denoted as \hat{n} . The lamp is placed along the z -axis, with the robotic arm moving along the x direction. Via integration along L , the total irradiation intensity generated with the lamp can be derived as

$$E = \frac{\Phi_E}{4\pi L \sqrt{x^2 + y^2}} \left(\text{atan} \left(\frac{\frac{L}{2} - z}{\sqrt{x^2 + y^2}} \right) + \text{atan} \left(\frac{\frac{L}{2} + z}{\sqrt{x^2 + y^2}} \right) \right) \hat{r} \cdot \hat{n} \quad (7)$$



(a)



(b)

Figure 8. An example of map generation for a laboratory environment using the RTABMap: (a) depth image and (b) 3D point cloud map.

The system can then obtain the total amount of irradiation for each location on the object by multiplying E with the time of exposure. Based on the discussions above, the algorithm developed for environmental disinfection is organized as follows:

Algorithm for environmental disinfection to achieve even disinfection for both the open area and objects in the environment:

Step 1: Activate the mobile robot manipulator to explore the environment and objects.

- Step 2: Generate the 2D map of the environment by using the Lidar and GMapping algorithm and the 3D map for the object in the environment by using the depth camera and RTABMap algorithm.
- Step 3: Navigate the mobile platform for disinfection in the open area. Conduct path planning for contour following of the object by using the PRM and NN algorithms and proceed with corresponding disinfection.
- Step 4: Estimate the UVC irradiation intensity for the locations on the object by using (7). If the intensity exceeds a preset value, move the robotic arm to the next disinfection location; otherwise, let it remain in the same location.
- Step 5: The process continues until the entire environment is fully disinfected.

The system is able to handle changes in room geometry via the sensors and navigation scheme. As for the case of human presence, the system would stop the disinfection process and send a message to the staff in charge if an individual has been detected in the restricted area.

2.4. Infection Risk Assessment

To evaluate how the risk of infection can be alleviated by introducing the proposed system, we came up with a quantitative assessment method based on the contact time and distance in a contagious environment, as they are positively related to infection risk. As the indoor social distance is set to be 1.5 m in Taiwan [39], it is regarded as effective contact for possible contagion when a person and source of infection are within that distance. Meanwhile, the risk of infection is considered to increase much more rapidly for a shorter distance. Consequently, we propose the infection risk rates for a confirmed case of contact between a robot $\alpha(d_c)$ and a person $\beta(d_c)$ to be formulated as

$$\alpha(d_c) = \left[e^{(d_c-1.5)^2} - 1 \right] \times \frac{1}{8.5} \quad (8)$$

$$\beta(d_c) = e^{(d_c-1.5)^2} - 1 \quad (9)$$

where d_c is the contact distance between a person and the source of infection, and their graphical demonstration is as shown in Figure 9. Here, the robot is still considered to be contagious, but to a lower degree. The value of 8.5 in (8) is used to place α between 0 and 1, and it can be smaller under a more strict disinfection process. With $\alpha(d_c)$ and $\beta(d_c)$ available, the index for infection risk R_c can be derived as

$$R_c = \frac{\int_0^{t_c} \alpha(d_c) \times t_c}{\int_0^{t_c} \beta(d_c) \times t_c} \times R_0 \quad (10)$$

where R_0 is the basic reproductive number, indicating how many people can be infected by one person without protection. This is with a median value at 5.7 [40], and t_c is the contact time when the contact distance is less than 1.5 m.

2.5. Real-Name System

Figure 10 shows the system diagram of the real-name system, which is installed in the fever station and linked with the proposed system to provide the necessary support. For instance, after temperature measurement, the system will send notices to the related personnel when someone is diagnosed. Information, including temperature, name, and photos with/without the mask, are recorded and stored in a database for further analysis. Users can also access the system with their mobile phone and generate a QR code for a given service, which takes place with a time limit to prevent embezzlement. To be further connected to more incoming intelligent systems developed in our university, the system is designed to be extensible.

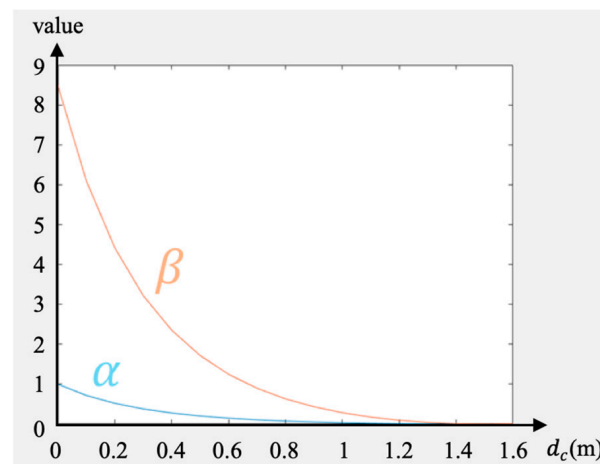


Figure 9. Graphical demonstration of $\alpha(d_c)$ and $\beta(d_c)$ relative to contact distance d_c .

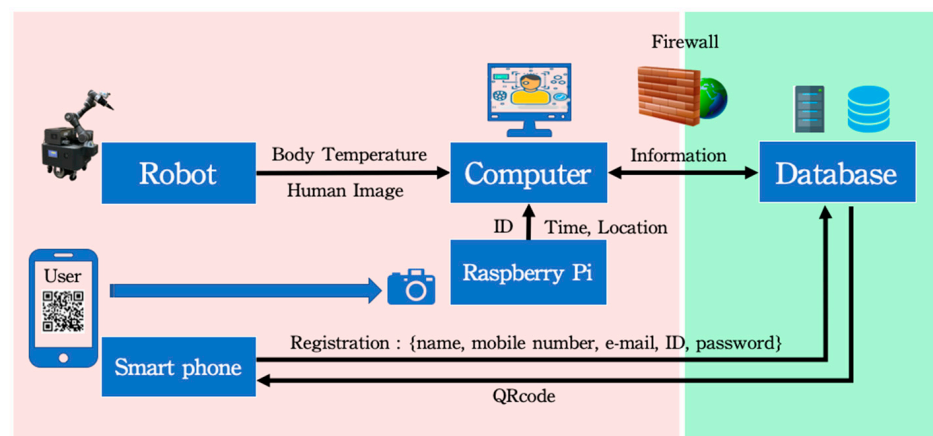


Figure 10. System diagram for the real-name system installed in the fever station.

3. Experiments

We conducted a series of experiments to evaluate the performance of the proposed system in the National Yang Ming Chiao Tung University (NYCU) intelligent ward, which was completed in 2020 and designed specifically for testing the intelligent medical systems developed by research teams in our university. The experiments have been approved by the IRB: NYCU-REC-111-087E. As shown in Figure 11, it includes the fever station, nursing station, and isolation ward, among others. A total number of 32 subjects, 20 males and 12 females, were invited to participate in the experiments, with their ages ranging from 20 to 25, except for 4 between 50 and 55. Among them, 21 participants had knowledge of robotics. After the experiments, they were asked to fill out a questionnaire to obtain their responses. The TM5-700 6-axis robot manipulator, manufactured by Techman Robot, Taiwan, was adopted as the robotic arm, employing the MoveIt motion planning framework for motion planning and governing. To support real-time execution, the proposed system was equipped with a computer with an Intel Core i5-6500TE CPU (manufactured by Intel in the United States), an Nvidia GeForce GTX 1650/4GB (manufactured by Nvidia in the United States), and the Ubuntu 16.04 operating system (developed by Canonical in the United Kingdom), along with the ROS Kinetic. The 2D lidar utilized was the UTM-30LX-EW, manufactured by Hokuyo in Japan. The depth camera employed was the RealSense D435, manufactured by Intel in the United States. The mobile platform utilized a differential drive system, designed and assembled by ITRI in Taiwan. UVC lamps, including the TUV G15 T8 and TUV G4 T5, were manufactured by Philips in the Netherlands. Please refer to the supplementary materials link for the experimental videos.



Figure 11. The NYCU intelligent ward is designed to have a hospital-like setting.

The first set of experiments was intended for temperature measurement in the fever station, with 17 subjects participating. As shown in Figure 12, when the system detected that a subject was sitting still on the chair, it started to navigate the mobile robot manipulator to come closer, governed the robotic arm, which was equipped with a non-contact infrared sensor, to approach his/her forehead to measure the temperature, and then sprayed alcohol to disinfect the hands. For these actions, the safety and comfort of the subject were deemed to be the main concerns. Figure 13a shows the distance between the subject and the robotic arm during the process, and Figure 13b shows its approaching speed. The robotic arm initially operated at a standard speed of 0.3 m/s. It began decelerating after 19 s when it was 40 cm away from the subject, marking the warning region. Eventually, it came to a halt at 13 cm in front of the subject's forehead, the predetermined measurement location, by the 22 s mark. After measurement, the robot conducted disinfection at 25 s and then started to return to the base at 37 s with the normal speed. From the experimental results for the 17 subjects, the system successfully completed the task for all cases with their safety and comfort ensured.

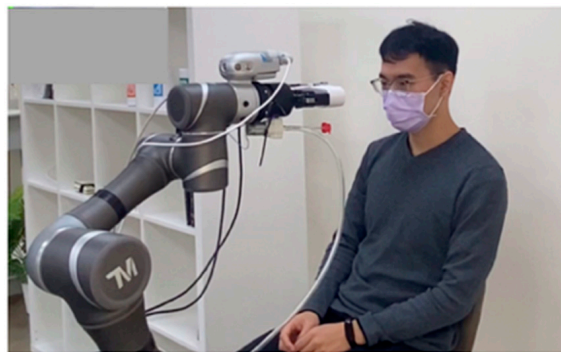


Figure 12. Experiment 1: temperature measurement.

The second set of experiments was intended for medicine delivery and taking in the isolation ward, with 15 subjects participating. As shown in Figure 14, the system first navigated the mobile robot manipulator to the nursing station to take the medicine, and then toward the bedside for its delivery. After delivery, the system would keep reminding the subject to take the medicine until it confirmed that he/she had actually taken the medicine by utilizing the algorithm for medicine-taking detection in Section 2.1. Same as

that shown in Experiment 1, the robot speed was regulated according to the relative distance between the subject and the robot. The task was executed successfully for all 15 subjects, demonstrating that the system was capable of delivering medicine while making sure that it had been taken.

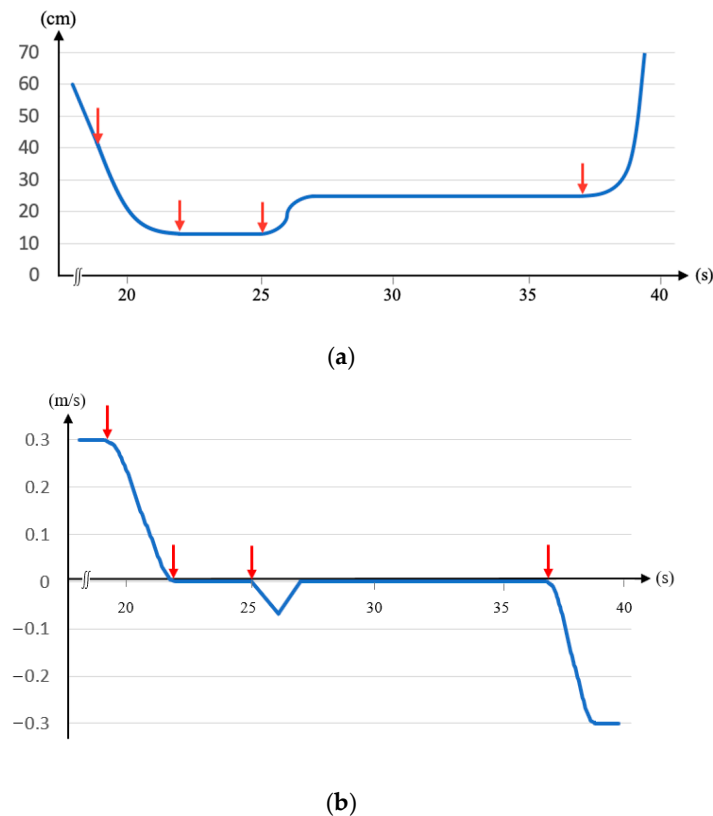


Figure 13. Results for Experiment 1: (a) distance between the subject and robotic arm and (b) approaching speed of the robotic arm.

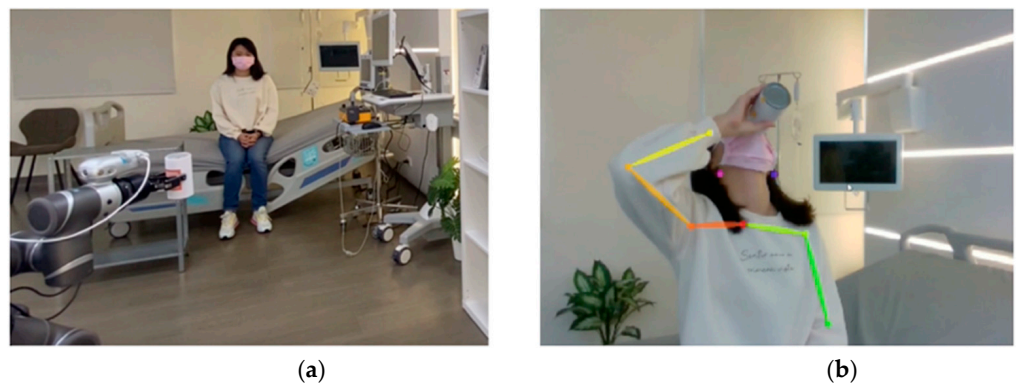


Figure 14. Experiment 2: (a) medicine delivery and (b) medicine taking.

The third set of experiments was intended to investigate whether the proposed system could achieve a more even disinfection effect in the presence of various kinds of objects in the environment. To provide a comparison, experiments were carried out utilizing the conventional method. This involved solely driving the mobile platform of the robot manipulator along a predetermined path for disinfection without engaging the robotic arm. In contrast, via the algorithm for environmental disinfection in Section 2.3 with the desired irradiation intensity value set at 22 mJ/cm [41], the proposed system would further maneuver the robotic arm to follow the contour of the object. Figure 15 shows an experimental scene in which five UVC dose cards (UVC 254 Tri Card, Intellego Technologies,

Sweden) used for irradiation intensity measurement were placed on several pieces of furniture in the smart ward. Table 1 lists the UVC dose readings on the five cards after both systems completed the disinfection process. Under the condition that almost the same amount of irradiation power was emitted from the UVC lamps for both systems, all the readings for the proposed system were larger than those of the conventional one, and they were all close to 22 mJ/cm, implying that the proposed system indeed achieved a more even disinfection effect.



Figure 15. Experiment 3: five UVC dose cards are placed on the furniture in the smart ward.

Table 1. Readings of UVC dose cards (mJ/cm²).

| Dose Card | Proposed System | Conventional System |
|-----------|-----------------|---------------------|
| 1 | 20 | 0 |
| 2 | 25 | 10 |
| 3 | 20 | 5 |
| 4 | 25 | 15 |
| 5 | 20 | 10 |

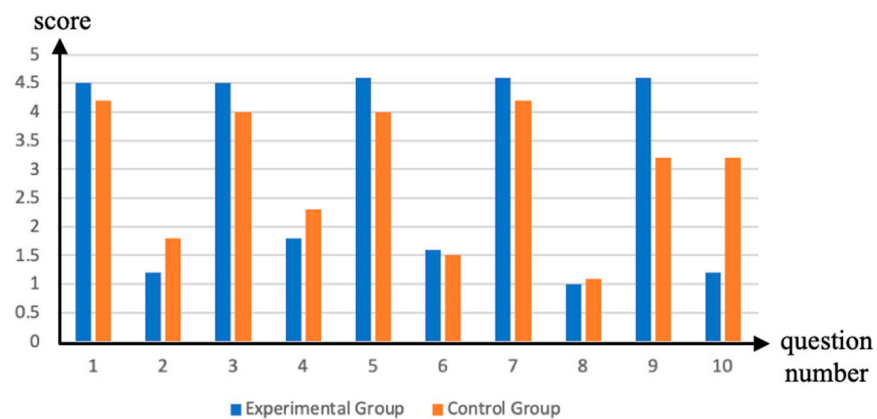
To evaluate how much possible infection risk might be reduced by replacing human personnel with the proposed system, we let the proposed system execute the tasks of temperature measurement and medicine delivery ten times, during which the robot navigated around the fever station, nursing station, and isolation ward. The whole process took about 85 s. The average risk infection index R_c , defined in Section 2.4, was computed to be 0.38 by using (10) according to the traveled distances that were within a contact distance of 1.5 m and their corresponding contact time. Compared to the basic reproductive number R_0 for COVID-19 at 5.7 [40], it showed a high potential for reducing infection risk by introducing robots for contagious diseases.

The questionnaire was conducted after the experiments to obtain subjects' feedback. The questions, listed in Table 2, were designed based on the system usability scale (SUS) [22], which is frequently used for evaluating human–machine systems. There were ten questions to be answered with a 5-item Likert scale [42]. The answers were collected and analyzed to yield a final SUS score, with a higher one indicating that the subject favors the selection more. For temperature measurement, the proposed system was compared with that of the fixed device commonly used in our society. In a traditional setup, subjects were required to approach the device closely to measure their temperature themselves. For medicine delivery, it was compared with the case of the medicine being delivered to the door of the isolation ward for the subjects to pick up. The average SUS scores for temperature measurement and medicine delivery were 90 vs. 74 and 83 vs. 58, respectively, indicating the subjects preferred the proposed system more. The detailed average scores for each question are shown in Figure 16, where the experimental group is with the proposed system and the control group is with the comparison system. From the follow-up interview, most

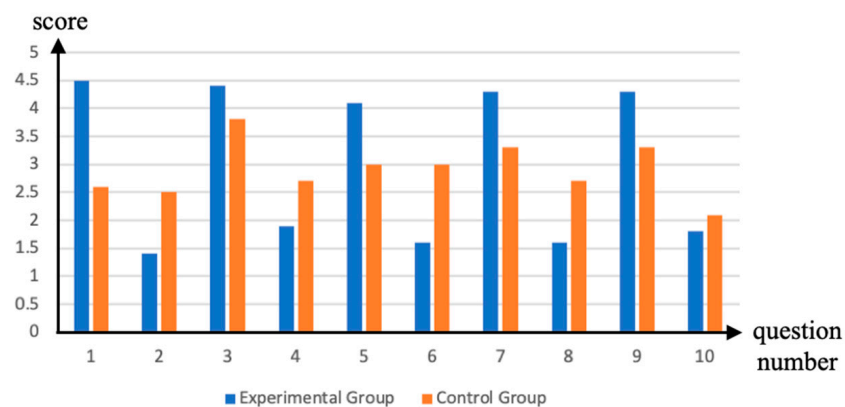
subjects expressed their acceptance of robots for medical services and showed appreciation for the autonomy they had brought in.

Table 2. Questions for the questionnaire.

| | Questions | Strongly Disagree | | Strongly Agree | |
|-----|--|-------------------|--|----------------|--|
| | | | | | |
| 1. | I think I am willing to use this system in the fever station (isolation ward). | | | | |
| 2. | I think the use of this system in the fever station (isolation ward) is too complicated. | | | | |
| 3. | I think this system is easy to use. | | | | |
| 4. | I think I need help to use this system. | | | | |
| 5. | I think the functions of this system are well integrated. | | | | |
| 6. | I think there are too many inconsistencies in this system. | | | | |
| 7. | I think most people can learn to use this system soon. | | | | |
| 8. | I think this system is troublesome to use. | | | | |
| 9. | I am confident that I can use this system. | | | | |
| 10. | I need to learn a lot of extra information to use this system. | | | | |



(a)



(b)

Figure 16. SUS score for (a) fever station and (b) isolation ward.

4. Conclusions

In this paper, we have proposed an autonomous fever detection, medicine delivery, and environmental disinfection system based on a mobile robot manipulator, which includes the functions of posture and action recognition, disinfection, safety control, infection

risk assessment, navigation, and real-name system. To ensure human safety and comfort, speed control was employed according to the relative distance between a human and a robot. An infection risk assessment was also executed to investigate the effect induced via robot introduction. A series of experiments were conducted at a hospital-like smart ward in our university for performance evaluation. The experimental results, as well as feedback from the subjects, have demonstrated its effectiveness. In future works, we plan to enhance the system to tackle various kinds of tasks in the hospital so that more medical personnel can be freed from infection threats.

Supplementary Materials: Please find the connection to the video that shows the experiments conducted above at <https://youtu.be/RcSiwraTV1w> (accessed on 16 December 2023).

Author Contributions: Conceptualization, C.-Y.S. and K.-Y.Y.; methodology, C.-Y.S. and K.-Y.Y.; software, C.-Y.S.; validation, K.-Y.Y.; writing—original draft, C.-Y.S. and K.-Y.Y. All authors have read and agreed to the published version of the manuscript.

Funding: This work was financially supported in part by the National Science and Technology Council, Taiwan, under grant NSTC 111-2221-E-A49-178-MY2.

Institutional Review Board Statement: The experiments have been approved by the IRB: NYCU-REC-111-087E.

Informed Consent Statement: Informed consent was obtained from all subjects involved in the study.

Data Availability Statement: The data presented in this study are available on request from the corresponding author. The data are not publicly available due to privacy.

Acknowledgments: The authors would also like to thank Guan-Ru Ou, Kai-Hsuan Shih, and Shun-Chia Yang for their assistance in the experiment execution.

Conflicts of Interest: The authors declare no conflict of interest.

References

1. Lanfranco, A.R.; Castellanos, A.E.; Desai, J.P.; Meyers, W.C. Robotic surgery: A current perspective. *Ann. Surg.* **2004**, *239*, 14. [[CrossRef](#)] [[PubMed](#)]
2. Szymona, B.; Maciejewski, M.; Karpiński, R.; Jonak, K.; Radzikowska-Büchner, E.; Niderla, K.; Prokopiak, A. Robot-assisted autism therapy (RAAT). Criteria and types of experiments using anthropomorphic and zoomorphic robots. Review of the research. *Sensors* **2021**, *21*, 3720. [[CrossRef](#)] [[PubMed](#)]
3. Schroeter, C.; Mueller, S.; Volkhardt, M.; Einhorn, E.; Huijnen, C.; van den Heuvel, H.; van Berlo, A.; Bley, A.; Gross, H.-M. Realization and user evaluation of a companion robot for people with mild cognitive impairments. In Proceedings of the 2013 IEEE International Conference on Robotics and Automation, Karlsruhe, Germany, 6–10 May 2013; pp. 1153–1159.
4. Yang, G.; Lv, H.; Zhang, Z.; Yang, L.; Deng, J.; You, S.; Du, J.; Yang, H. Keep healthcare workers safe: Application of teleoperated robot in isolation ward for COVID-19 prevention and control. *Chin. J. Mech. Eng.* **2020**, *33*, 1–4. [[CrossRef](#)]
5. Conte, D.; Leamy, S.; Furukawa, T. Design and map-based teleoperation of a robot for disinfection of COVID-19 in complex indoor environments. In Proceedings of the 2020 IEEE International Symposium on Safety, Security, and Rescue Robotics (SSRR), Abudhabi, United Arab Emirates, 4–6 November 2020; pp. 276–282.
6. Mišeikis, J.; Caroni, P.; Duchamp, P.; Gasser, A.; Marko, R.; Mišeikienė, N.; Zwilling, F.; De Castelbajac, C.; Eicher, L.; Früh, M. Lio—a personal robot assistant for human-robot interaction and care applications. *IEEE Robot. Autom. Lett.* **2020**, *5*, 5339–5346. [[CrossRef](#)] [[PubMed](#)]
7. Cao, Y.; Li, Q.; Chen, J.; Guo, X.; Miao, C.; Yang, H.; Chen, Z.; Li, C.; Li, L. Hospital emergency management plan during the COVID-19 epidemic. *Acad. Emerg. Med.* **2020**, *27*, 309–311. [[CrossRef](#)] [[PubMed](#)]
8. Huang, H.-W.; Chen, J.; Chai, P.R.; Ehmke, C.; Rupp, P.; Dadabhoy, F.Z.; Feng, A.; Li, C.; Thomas, A.J.; da Silva, M. Mobile robotic platform for contactless vital sign monitoring. *Cyborg Bionic Syst.* **2022**, *2022*, 9780497. [[CrossRef](#)] [[PubMed](#)]
9. Rane, K.P. Design and development of low cost humanoid robot with thermal temperature scanner for COVID-19 virus preliminary identification. *Int. J.* **2020**, *9*, 3485–3493. [[CrossRef](#)]
10. Kim, R. Development of an autonomously navigating robot capable of conversing and scanning body temperature to help screen for COVID-19. In Proceedings of the 2021 IEEE MIT Undergraduate Research Technology Conference (URTC), Cambridge, MA, USA, 8–10 October 2021; pp. 1–5.
11. Nakhaeina, D.; Laferrière, P.; Payeur, P.; Laganière, R. Safe close-proximity and physical human-robot interaction using industrial robots. In Proceedings of the 2015 12th Conference on Computer and Robot, Vision, Halifax, NS, Canada, 3–5 June 2015; pp. 237–244.

12. Lasota, P.A.; Rossano, G.F.; Shah, J.A. Toward safe close-proximity human-robot interaction with standard industrial robots. In Proceedings of the 2014 IEEE International Conference on Automation Science and Engineering (CASE), New Taipei, Taiwan, 18–22 August 2014; pp. 339–344.
13. Rosenstrauch, M.J.; Krüger, J. Safe human-robot-collaboration-introduction and experiment using ISO/TS 15066. In Proceedings of the 2017 3rd International Conference on Control, Automation and Robotics (ICCAR), Nagoya, Japan, 24–26 April 2017; pp. 740–744.
14. Donovan, J.L.; Blake, D.R. Patient non-compliance: Deviance or reasoned decision-making? *Soc. Sci. Med.* **1992**, *34*, 507–513. [[CrossRef](#)]
15. Kleinsinger, F. The unmet challenge of medication nonadherence. *Perm. J.* **2018**, *22*, 18–33. [[CrossRef](#)]
16. Lee, H.; Youm, S. Development of a wearable camera and AI algorithm for medication behavior recognition. *Sensors* **2021**, *21*, 3594. [[CrossRef](#)]
17. Jun, K.; Oh, S.; Lee, D.-W.; Kim, M.S. Management of medication using a mobile robot and artificial intelligence. In Proceedings of the 2021 IEEE Region 10 Symposium (TENSYP), Jeju, Republic of Korea, 23–25 August 2021; pp. 1–3.
18. Osawa, R.; Huang, S.Y.; Yu, W. Development of a Medication-Taking Behavior Monitoring System Using Depth Sensor. In Proceedings of the International Conference on Intelligent Autonomous Systems, Suwon, Republic of Korea, 4–7 July 2021; pp. 250–260.
19. Datta, S.; Karmakar, C.K.; Palaniswami, M. Averaging methods using dynamic time warping for time series classification. In Proceedings of the 2020 IEEE Symposium Series on Computational Intelligence (SSCI), Canberra, Australia, 1–4 December 2020; pp. 2794–2798.
20. Tiseni, L.; Chiaradia, D.; Gabardi, M.; Solazzi, M.; Leonardis, D.; Frisoli, A. UV-C mobile robots with optimized path planning: Algorithm design and on-field measurements to improve surface disinfection against SARS-CoV-2. *IEEE Robot. Autom. Mag.* **2021**, *28*, 59–70. [[CrossRef](#)]
21. Sanchez, A.G.; Smart, W.D. Verifiable Surface Disinfection Using Ultraviolet Light with a Mobile Manipulation Robot. *Technologies* **2022**, *10*, 48. [[CrossRef](#)]
22. Brooke, J. Sus: A “quick and dirty” usability. *Usability Eval. Ind.* **1996**, *189*, 189–194.
23. Su, C.-Y.; Wang, H.-C.; Ko, C.-H.; Young, K.-Y. Development of an Autonomous Robot Replenishment System for Convenience Stores. *Electronics* **2023**, *12*, 1940. [[CrossRef](#)]
24. Cao, Z.; Hidalgo, G.; Simon, T.; Wei, S.E.; Sheikh, Y. OpenPose: Realtime Multi-Person 2D Pose Estimation Using Part Affinity Fields. *IEEE Trans. Pattern Anal. Mach. Intell.* **2021**, *43*, 172–186. [[CrossRef](#)] [[PubMed](#)]
25. Gu, J.; Wang, Z.; Kuen, J.; Ma, L.; Shahroudy, A.; Shuai, B.; Liu, T.; Wang, X.; Wang, G.; Cai, J. Recent advances in convolutional neural networks. *Pattern Recognit.* **2018**, *77*, 354–377. [[CrossRef](#)]
26. Hearst, M.A.; Dumais, S.T.; Osuna, E.; Platt, J.; Scholkopf, B. Support vector machines. *IEEE Intell. Syst. Their Appl.* **1998**, *13*, 18–28. [[CrossRef](#)]
27. Charalambous, G.; Fletcher, S.; Webb, P. Identifying the key organisational human factors for introducing human-robot collaboration in industry: An exploratory study. *Int. J. Adv. Manuf. Technol.* **2015**, *81*, 2143–2155. [[CrossRef](#)]
28. Koppenborg, M.; Nickel, P.; Naber, B.; Lungfiel, A.; Huelke, M. Effects of movement speed and predictability in human-robot collaboration. *Hum. Factors Ergon. Manuf. Serv. Ind.* **2017**, *27*, 197–209. [[CrossRef](#)]
29. Connor UVC Disinfection Robot. Available online: <https://www.robotlab.com/store/connor-uvc-disinfection-robot> (accessed on 7 December 2023).
30. LightStrike Pulsed, High Intensity, Broad Spectrum UV Light Devices. Available online: <https://xenex.com/light-strike> (accessed on 7 December 2023).
31. Intelligent Disinfection Robot. Available online: <http://www.tmirob.com/solutions/19> (accessed on 7 December 2023).
32. XDBot. Available online: <https://www.transformarobotics.com/xdbot> (accessed on 7 December 2023).
33. Intelligent Disinfection Robots Help Fight the Virus. Available online: <https://www.siemens.com/global/en/company/stories/industry/intelligentrobotics-siemens-aucma.html> (accessed on 7 December 2023).
34. Grisetti, G.; Stachniss, C.; Burgard, W. Improving grid-based slam with rao-blackwellized particle filters by adaptive proposals and selective resampling. In Proceedings of the 2005 IEEE International Conference on Robotics and Automation, Barcelona, Spain, 18–22 April 2005; pp. 2432–2437.
35. Labbé, M.; Michaud, F. RTAB-Map as an open-source lidar and visual simultaneous localization and mapping library for large-scale and long-term online operation. *J. Field Robot.* **2019**, *36*, 416–446. [[CrossRef](#)]
36. Zhang, Y.; Zhang, L.; Lei, L.; Xu, F. An Improved Potential Field-Based Probabilistic Roadmap Algorithm for Path Planning. In Proceedings of the 2022 6th International Conference on Automation, Control and Robots (ICACR), Shanghai, China, 23–25 September 2022; pp. 195–199.
37. Takashima, Y.; Nakamura, Y. Theoretical and Experimental Analysis of Traveling Salesman Walk Problem. In Proceedings of the 2021 IEEE Asia Pacific Conference on Circuit and Systems (APCCAS), Penang, Malaysia, 22–26 November 2021; pp. 241–244.
38. Fredes, P.; Raff, U.; Gramsch, E.; Tarkowski, M. Estimation of the ultraviolet-C doses from mercury lamps and light-emitting diodes required to disinfect surfaces. *J. Res. Natl. Inst. Stand. Technol.* **2021**, *126*, 1–24. [[CrossRef](#)]
39. Taiwan Center for Disease Control. Available online: <https://www.cdc.gov.tw/En> (accessed on 1 November 2023).
40. Sanche, S.; Lin, Y.T.; Xu, C.; Romero-Severson, E.; Hengartner, N.; Ke, R. High contagiousness and rapid spread of severe acute respiratory syndrome coronavirus 2. *Emerg. Infect. Dis.* **2020**, *26*, 1470. [[CrossRef](#)] [[PubMed](#)]

41. Weyersberg, L.; Sommerfeld, F.; Vatter, P.; Hessling, M. UV radiation sensitivity of bacteriophage PhiX174-A potential surrogate for SARS-CoV-2 in terms of radiation inactivation. *AIMS Microbiol.* **2023**, *9*, 431–443. [[CrossRef](#)] [[PubMed](#)]
42. Joshi, A.; Kale, S.; Chandel, S.; Pal, D.K. Likert scale: Explored and explained. *Br. J. Appl. Sci. Technol.* **2015**, *7*, 396–403. [[CrossRef](#)]

Disclaimer/Publisher’s Note: The statements, opinions and data contained in all publications are solely those of the individual author(s) and contributor(s) and not of MDPI and/or the editor(s). MDPI and/or the editor(s) disclaim responsibility for any injury to people or property resulting from any ideas, methods, instructions or products referred to in the content.